NANO LETTERS

2007
Vol. 7, No. 6
1664−1669

Gold Nanoparticle Growth Monitored in situ Using a Novel Fast Optical Single-Particle Spectroscopy Method

Jan Becker, Olaf Schubert, and Carsten Sönnichsen*

Institute for Physical Chemistry, University of Mainz, Jakob-Welderweg 11, 55128 Mainz, Germany

Received March 16, 2007; Revised Manuscript Received April 12, 2007

ABSTRACT

Size- and shape-dependent optical properties of gold nanorods allow monitoring their growth using a novel fast single-particle spectroscopy (fastSPS) method. FastSPS uses a spatially addressable electronic shutter based on a liquid crystal device to investigate particles randomly deposited on a substrate, orders of magnitude faster than other techniques. We use fastSPS to observe nanoparticle growth in situ on a single-particle level and extract quantitative data on nanoparticle growth.

Large-scale and inexpensive production of nanoparticles by chemical solution based synthesis allows the use of the unique properties of nanoscale materials for a variety of new materials, devices, and as a versatile research tool.[1,2] Among the most striking optical small-size effects are fluorescence due to quantum confinement (quantum dots)[3] and light scattering due to electrodynamic resonances (plasmons).[4] It is now routinely possible to produce inorganic crystalline nanoparticles of various shapes and sizes.[5−7] Compared to the atomic level of control achievable in organic synthesis, the wet chemical production of nanoparticles often suffers from low yield and/or a relatively broad size and shape distribution. Circumventing the issue of inhomogeneous samples, microscopic techniques to study optical properties of *individual* nanoparticles have become a major characterization tool.[8] In addition, single-particle microscopy allows the fabrication of nanoscale devices such as sensors with ultimate miniaturization[9,10] and the use of particles for biolabeling applications.[11−13] Besides resolution and sensitivity, obtaining enough statistics within a reasonable time frame on inhomogeneous samples is a major issue in single-particle characterization techniques. The origin of the inhomogeneous growth of nanoparticle samples and details of the growth mechanism are not well understood in most cases.[14] The study of the particle growth process itself on a single-particle level has so far been limited due to difficulties in obtaining enough statistics and due to technical complexity. Most studies rely on stopping the reaction at various points and determine particle morphology at aliquots taken at those times.[15−19]

Here, we present a novel fast single-particle spectroscopy method (fastSPS) based on an electronically addressable spatial shutter, which allows the simultaneous investigation of many particles with high temporal resolutions, fast enough to study nanoparticle growth on a single-particle level in real time and in situ. The method is presently at least an order of magnitude faster than the traditional serial measurement of one particle at a time assuming ideal implementation. The fastSPS method compares even more favorable under realistic conditions and has itself room for further improvement in speed. FastSPS uses no mechanical parts or sample movement, which potentially allows this method to become an inexpensive, sturdy system for use outside of a laboratory environment, for example, for medical sensoring applications.[9,20] We use fastSPS to study the growth process of rod-shaped gold nanoparticles in the presence of surfactant molecules and find that the particles grow mainly in the direction of the short rod axis, resulting in a decrease of the aspect ratio. This is, to the best of our knowledge, the first real-time optical observation of nanoparticle growth on a single-particle level. FastSPS will be useful for other real-time spectral monitoring applications such as the use of plasmon particles as labels in single-molecule studies.[11,20]

The key for our optical study of nanoparticle growth on a single-particle level is the fact that the light-scattering spectrum of gold nanorods depends delicately on size and shape.[6,21] The scattering spectrum is dominated by the long-axis plasmon resonance, which shifts toward longer wavelengths for higher aspect ratios[22] and broadens for larger particles due to increased radiation damping.[23] Hence, it is possible to deduce the particle shape and size by observing the resonance energy and line width of single particles,

* Corresponding author. E-mail: soennichsen@uni-mainz.de.

10.1021/nl070627g CCC: $37.00
Published on Web 05/02/2007

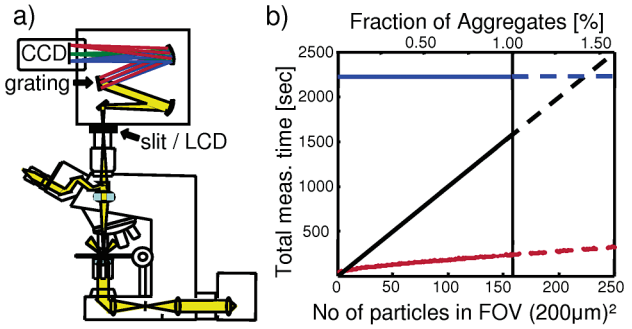

Figure 1. (a) Schematics of the dark-field microscope setup. The scattered light is directed either to the ocular or to an imaging spectrometer, where the light is dispersed and the resulting spectrum captured by a CCD camera. (b) For randomly deposited particles, higher particle densities on the sample (lower horizontal axis) lead to a higher percentage of more than one particle in a diffraction limited spot (particle aggregates, upper horizontal axis). The total measurement time for all particles in the field of view increases linearly for a serial method (black line) and is independent for all spectral imaging methods that determine the spectra of all points in the field of view (blue line). The fastSPS method (red line) is by far the fastest method for realistic particle densities around 160 particles in the field of view (200 μm)^2 corresponding to roughly 1% of particle aggregates.

assuming the particle shape is not drastically changed and the particle environment stays the same. In other words, the "phase space" of particle shape (size and aspect ratio) maps bijective onto the experimentally observable "phase space" of line widths and resonance energy.[24]

To optically observe single particles, we use a standard transmission type dark-field microscope[23,25,26] with a high numerical aperture condenser (NA 1.2−1.4) and a 40× air objective (NA 0.75) coupled with an imaging spectrometer (SP-2150i, Acton; grating: 300 gr/mm; spectral resolution: 1.6 nm) and read out by a peltier-cooled (−75 °C) back-illuminated charged-coupled device (CCD) camera (Pixis400, Princeton Instruments; 1340 × 400 pixels per (20 μm)^2), as shown in Figure 1a. The novel aspect is that we replace the entrance slit of the spectrometer by an electronically addressable liquid crystal device (LCD) (LC2002, Holoeye; 800 × 600 pixels (230 × 230 pixels used in our setup) with (32 μm)^2 pixel size; response time: 40 ms; the pixel size corresponds to the diffraction-limited spot of one nanoparticle magnified by our 40× objective). LCDs are currently used in a variety of optical setups including optical-sectioning fluorescence spectroscopy[27] and speckle-illuminated confocal fluorescence microscopy,[28] but have, to the best of our knowledge, not been used as a spatial addressable shutter for spectrometers. We place the LCD in the image plane of the microscope so that each of its pixels corresponds to a distinct point in the focal plane of the objective and effectively acts as an individual electronically addressable shutter for this area. The LCD is at the same time in the entrance plane of an imaging spectrometer. By setting an LCD pixel to transparent, a corresponding particle is spectrally investigated. Currently, the spectrometer allows the imaging of up to 20 vertically separated spectra on the CCD chip before overlap between spectra becomes problematic. By using more sophisticated spectrometer optics, we expect to improve this value considerably in a future system.

In a standard measurement, we first set all LCD pixels to transparent and take a black-and-white image of the whole sample by moving the spectrometer grating to zero's order. In principle, a second camera attached to another output port of the microscope could be used for this as well, which would further speed up the measurement. N Nanoparticles are then selected by hand or by setting a threshold. The nanoparticle positions (X_i, Y_i) are arranged into n nonhorizontally overlapping groups (G^n) of up to 20 particles. Each group (G^n) is then measured consecutively by setting the corresponding pixels to transparent. The resulting images (I^n) are decomposed into the particle spectra (S_i), taking into account a small wavelength shift due to the horizontal position offset ($X_i - X_c$) from the center of the spectrometer entrance (X_c). A dark image (I^0), taken by setting all pixels to black, can be subtracted from all images (I^n) to account for light leaking through black LCD pixels despite the >1:1000 contrast achievable with LCD displays. Furthermore, the spectra (S_i) need to be corrected for background from diffuse light originating from out-of-focus areas of the sample, i.e., dust on the glass surface. Therefore, one additional spectrum (S_0) from a point of the sample without a particle is measured and subtracted from each particle spectrum (S_i). Finally, the spectra are normalized to the spectral characteristic determined for a "white" particle (W), either dust or large silicon dioxide beads, $S_{final} = (S_i - S_0)/W$. The stability of the setup, determined by observing a single particle continuously for about 3 h, shows subnanometer deviations (see Supporting Information Figure S1) limited mainly by focus drift.

To compare the speed of our new fastSPS method with other methods for spectrally investigating particles in a microscope, it is important to realize that the density of randomly deposited particles on the substrate is necessarily low in single-particle studies. Because the diffraction limit makes it impossible to reliably distinguish two particles from a single particle if they are closer than the current resolution, the only way to investigate single particles (on average) is to dilute them on the substrate up to a point where it is very unlikely to find two particles in the same diffraction limited spot. The probability p of such "aggregates" is given by $p = 1 - (1 - N/M)^m$ with N the number of particles in the field of view, M the number of "absorption areas" in this field of view, assuming that one absorption area has the size of one nanoparticle and m is the size of the optical resolution as a multiple of the absorption area. p increases to more than 1% of the deposited particles for densities around 160 particles in the field of view of (200 μm)^2 assuming a resolution of 900 nm (Figure 1b). Any method measuring the spectra of each point in the field of view ("spectral imaging") produces therefore a vast amount of unnecessary data. Several technical possibilities exist for realizing such a spectral imaging approach, from scanning the illumination wavelength,[29] using an interferometric approach[30] to moving the sample relative to the entrance slit of the spectrometer.[31,32]

Depending on particle density, automatization grade, speed of sample movement, etc., the more traditional "serial" approach of investigating exactly the particle in the center of view and positioning all particles of interest in this spot consecutively[11] is usually faster for low particle densities. Figure 1b numerically compares our fastSPS approach with a spatial addressable shutter to the serial and spectral imaging method for different particle densities. In addition, we have experimentally compared fastSPS with spectral imaging realized by moving the spectrometer with a fixed entrance slit relative to the sample with a stepper motor (data not shown). Both simulation and experiment show at least an order of magnitude faster spectra acquisition time for realistic particle densities of about 160 particles per (200 μm)^2. We have adjusted the exposure time of the fastSPS method in these calculations to account for light blocked by the LCD's polarization filters (about 50% of the incoming light). It will be, however, relatively simple to circumvent this issue by splitting the light into two optical pathways of orthogonal polarization with a polarizing beam splitter and using two LCD displays. In this improved configuration, currently under construction, not only spectral but also orientation information is gained, which can be used to extract particle orientation of optically anisotropic particles.[25,33]

We use the fastSPS method to investigate nanoparticle growth, specifically gold nanorods in a "growth solution" containing gold ions and surfactant molecules. The interest in this system originates in the recent observation of a change in particle growth mode from one to three dimensional on particles grown in a continuous flow reactor.[34] We first synthesize small gold nanorods in a batch synthesis according to literature procedure[6] by adding small spherical gold seeds to a growth solution containing gold ions, silver ions in a ratio of 6.25:1, a mild reducing agent (ascorbic acid) and a surfactant (cetyl-trimethyl-ammonium bromide, CTAB). Figure 2a shows a transmission electron microscope (TEM) image of the rods used in this work. Statistical image analysis of 160 rods results in a mean length of 48 $\pm$ 4 nm, a mean width of 22 $\pm$ 3 nm, and a mean aspect ratio of 2.2 $\pm$ 0.3.

Before investigating single particles, we perform a batch control experiment by diluting 50 μL of the above rod solution in 950 μL of CTAB (0.1M). After 10 min, we add 1000 μL of a double concentrated growth solution containing twice the amount of gold, silver, and ascorbic acid compared to the literature values in order to get the normal values in the final reaction mix. The rods are incubated for $2^1/_2$ h, at which point, we take TEM images of the resulting particles (Figure 2b). Statistical analysis of 160 particles yields a mean length of 97 $\pm$ 12 nm, a mean width of 73 $\pm$ 12 nm, and a mean aspect ratio of 1.4 $\pm$ 0.2. The extinction spectrum of the particle growth process is continuously monitored with a fiber spectrometer (see Supporting Information Figure S3) and shows a shift in peak extinction wavelength from 636 to 597 nm in the course of the reaction. This batch experiment is not directly comparable to particle growth near surfaces but shows the general trend that we expect for particle growth under these conditions: mainly in the direction of the short axis.

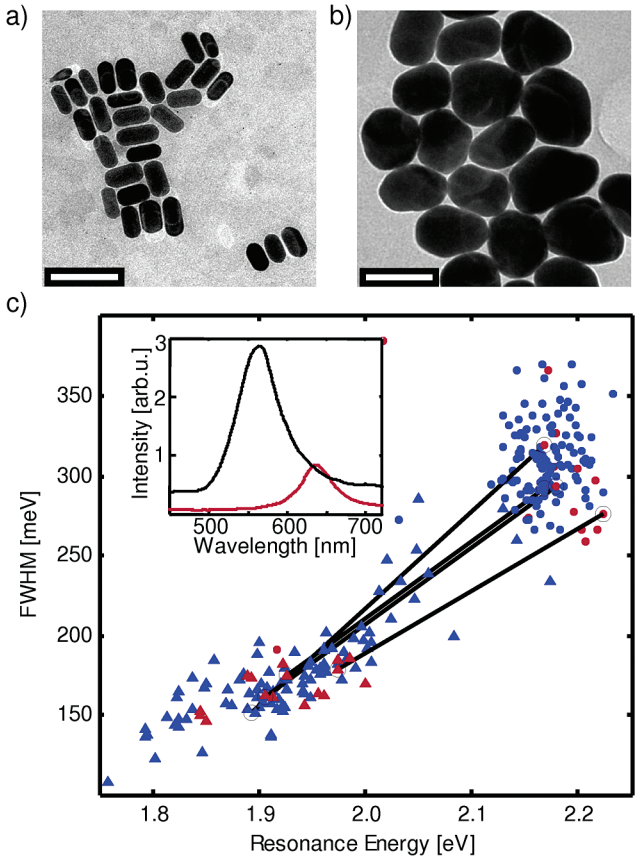

Figure 2. (a) TEM image of original gold nanorod sample. (b) TEM image of the sample after $2^1/_2$ h incubation in growth solution in a batch experiment. The particles are considerably larger and more spherical. Scale bars are 100 nm. (c) Optical single-particle spectra of particles before (triangles) and after (dots) rinsing them with growth solution for about 180 min. For each spectrum, the full width at half-maximum (fwhm) is plotted against the resonance energy. The particles corresponding to the red markers are continuously measured. The inset shows an example of a single-particle spectrum before (red) and after (black) rinsing with growth solution. The increase of absolute intensity is caused by the increased particle volume.

To investigate the growth on a single-particle level, we dilute the rod−solution 1:100 with distilled water and rinse them for 5 min through a flow-cell consisting of a thin, flat glass capillary (0.1 mm × 2 mm × 100 mm) connected to PET tubing. Some of the rods stick to the glass surface, which is enhanced by addition of small amounts of sodium chloride. When enough rods are immobilized in the field of view, we rinse with pure CTAB (0.1M) and measure the spectra of all particles in this field of view. About 20 of those particles are now continuously monitored in parallel for about 165 min every 30 s. We replace the pure CTAB rinsing solution after 10 min with a growth solution containing 1/10 of the standard values of gold, silver, and ascorbic acid and rinse for about $2^1/_2$ h. The amount of gold ions in relation to the number of particles is chosen to match the batch experiment, which leads, however, to a slower reaction kinetics because of the lower absolute concentration. Figure 2c shows the full width at half-maximum (fwhm) of each spectrum against its resonance energy at the start of the experiment (triangles) as well as at the end (dots). Both the

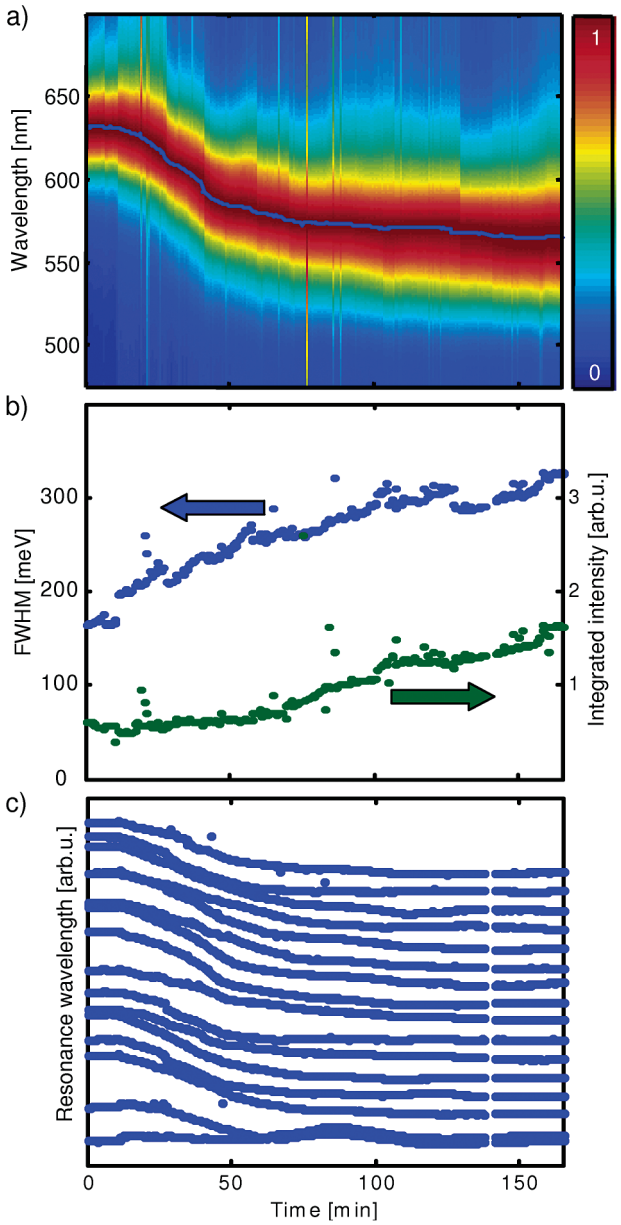

Figure 3. (a) Normalized scattering spectra of one single particle during rinsing with growth solution shown as color-coded as a function of time. During the first 10 min, the particle is incubated in pure CTAB solution (0.1 M). For the same measurement, the time development of the fwhm (blue dots) and the integral of intensity over the wavelengths (green dots) are shown in (b). The resonance wavelength of 16 particles from one experimental run is shown as a function of time (with an arbitrary offset) in (c). The upper 14 lines show particles where the resonance wavelengths develop similarly, while the lowest two lines shows particle with a nearly constant resonance wavelength.

resonance energy of the particles and the fwhm increases, confirming that the aspect ratio of the particles decreases and the overall size increases. The red dots represent 16 of the particles investigated continuously during rinsing with growth solution. The inset shows the full spectra of one single particle before (red) and after (black) rinsing with the growth solution, where we see, in addition to the shifts in line width and resonance energy, a considerable increase in peak intensity, which we will discuss below.

For one of the 20 particles observed continuously, the resulting spectra are shown (color coded) as a function of time in Figure 3a. Figure 3b shows the development of the fwhm of the same particle (left axis) and the (integrated) scattered light intensity (right axis). Initially, there is a constant period where the particles are incubated in pure CTAB solution. A small step-like change in the fwhm and intensity occurs at the start of the rinsing process, a phenomenon previously observed[11] and currently unexplained. During rinsing with growth solution, the fwhm increases nearly linear over time (the steps after about 28, 58, and 127 min are due to refocusing). The intensity of the scattered light integrated over all wavelengths (I_{sca}) increases strongly over time. Because I_{sca} scales, in general, with the square of the particle volume, the increase shows the overall particle growth. The scaling of I_{sca} with the square of the particle volume is, however, not strictly applicable for plasmon resonant particles, because a shift in resonance energy and/or the amount of damping may also have some effect.[23,35] Figure 3c shows the development of the resonance wavelength of 16 particles investigated in parallel during rinsing with growth solution (four particles turned out to be useless for analysis, for example, due to a dust particle setting down nearby during observation).

The measured optical scattering spectra of individual particles allow the direct deduction of particle size and shape. The particle shape is either described by the particle aspect ratio (a/b) and volume (V), or the dimensions of the particle's long (a) and short axis (b). In principle, the plasmon resonance position E_{res} and its line width Γ of a particle with a given geometry (e.g., cylindrical) and embedded in a given environment is directly connected with the geometrical parameters a and b (or a/b and V) via a bijective function F: $a,b \leftrightarrow E_{res},\Gamma$ converting optically measured values into particle size. This function F can be calculated by solving Maxwell's equations either analytically, e.g., using Mie's equations (for spherical particles) or numerically, for example by the method of discrete dipoles. We use a combination of values from Mie theory and discrete dipole simulations obtained with the software DDSCAT 6.1.[36] Our DDSCAT calculations were performed with dipole distances of 2 nm using a spherically capped cylinder as particle shape. For all calculations, we use the values for the dielectric function of gold as provided by Johnson and Christy.[37] The resulting form of the function F is shown in part in Figure 4a in a three-dimensional plot (the discrete points used for the extrapolation are listed in Table S1 in the Supporting Information). We also indicate the trajectory of one particle in this space. The resulting particle geometry evolution is shown in Figure 4b. Because the measured spectral width is very sensitive to defocusing, the resulting particle geometry data are relatively noisy and show jumps at points in time where we refocused.

An alternative to the method used above is the use of the scattered light intensity I_{sca} (at the maximum) as the second experimental parameter instead of the fwhm. The time dependence of I_{sca} is easily extracted from the measured data and shows a stronger increase over the course of the particle

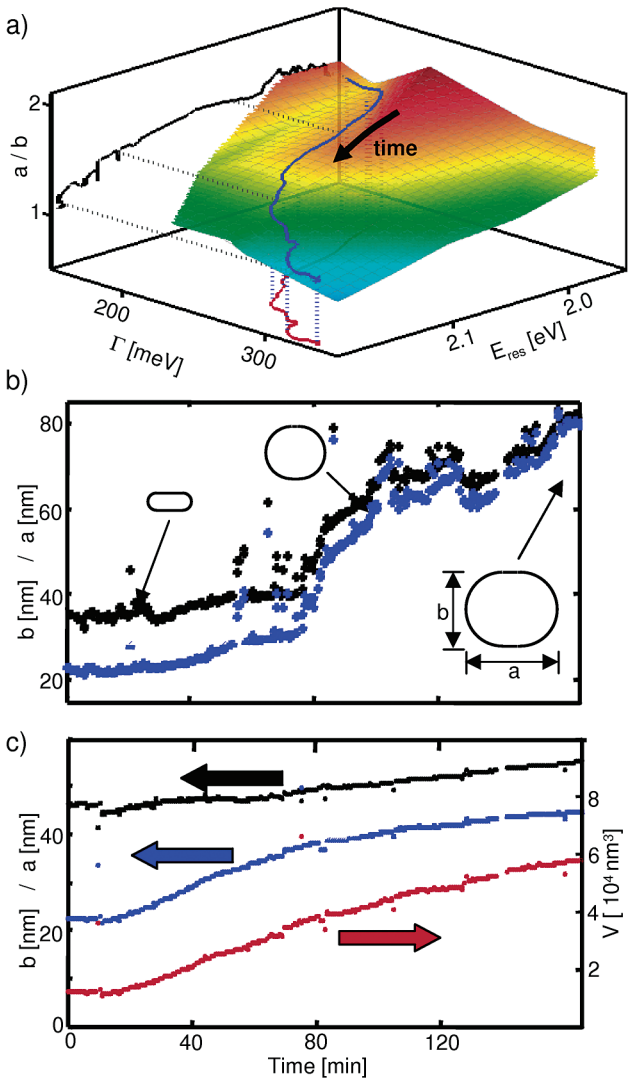

Figure 4. (a) The particle geometry (given by the long and short axes a and b, or the aspect ratio a/b and the volume V) are related to the measured spectral quantities resonance position (E_{res}) and line width (Γ) by a bijective function F (shown as colored surface area). The function F was calculated by interpolation between values obtained by DDA simulations and Mie calculations (see Supporting Information Table S1). We have indicated a measured trajectory of E_{res} and Γ (red line) and the corresponding trajectory of the aspect ratio (blue line). (b) Time development of the long (black)/short (blue) axis of one single nanorod as a function of time (respectively) as determined by the function F. The insets indicate the size of the rod at three moments in time. (c) Average shape development of 12 particles calculated from E_{res} and the measured scattering intensity I_{sca} by the simplified function G. The individual traces are shown in Figure S4 in the Supporting Information.

growth than the fwhm. The conversion of E_{res} and I_{sca} into particle size parameters a/b and V requires, however, the a priori knowledge of the initial particle size V_0. We use the average value of V_0, determined from TEM images (Figure 2a), as an approximation. By taking only the dependency of E_{res} on a/b into account, a/b is calculated by the empirically[38] derived formula $1240\ \text{eV}/E_{res} = (53.71\ a/b - 42.29)\ \varepsilon_m + 495.14$ with the dielectric permittivity of the surrounding medium $\varepsilon_m = (1.33)^2$. The relationship of V to I_{sca} and E_{res} follows from $I_{sca} \propto \lambda^{-4}|\alpha|^2$ with the complex polarizability α.[39] Using the quasistatic approximation to calculate α for ellipsoidal particles, we obtain for the intensity at the resonance wavelength λ_{res}

$$I(\lambda_{res}) \propto \frac{1}{\lambda_{res}^4}\left|\frac{1-\varepsilon'_r-i\varepsilon''_r}{i\varepsilon''_r}\right|^2 \cdot \frac{V^2}{L_a^2}$$

with the complex relative dielectric permittivity $\varepsilon_r = \varepsilon_{metal}/\varepsilon_{medium} = \varepsilon'_r + i\varepsilon''_r$ and L_a the shape parameter of the long axis approximately given by $L_a = (1 + a/b)^{-1.6}$ (ref 26). Figure S4 in the Supporting Information shows the development of the particle geometry of all 16 individual particles as derived from I_{sca} and E_{res}. The mean over those single-particle results are shown in Figure 4c.

Regardless of the method used to derive the particle size development, a faster growth of the short axis compared to the long particle axis is evident (Figure 4b,c). Even though the derivation of particle sizes using the line width is theoretically more elegant, the current limitations in the experimental accuracy favors the use of the second method, the derivation from the measured scattering intensity, and the resonance energy. The mean over several simultaneously measured particles shown in Figure 4c is an accurate description of the growth behavior of gold nanorods in the given environment. The volume increases linearly over time with a rate of about 5 nm^3/s, which is comparable to the rate expected from diffusion-limited growth. Thus, diffusion or mass transport limits the reaction in our case. Knowing the growth kinetics and the limiting step of the reaction will be useful for controlled particle growths on surfaces and in solution.

We believe that the novel fastSPS setup for the investigation of single-particle spectroscopy on several particles in parallel gives a very useful tool for spectral investigation of diluted samples if temporal resolution is critical. Currently, the method is at least an order of magnitude faster than other methods, and there is ample room for further improvement, i.e., by using more sophisticated imaging spectrometer. The fastSPS method (using an electronically addressable spatial shutter) requires no moving parts, which makes it, in principle, possible to implement it in small, robust future devices, i.e., for ultrasmall volume sensors "in the field". It may also be possible to use this method in other scientific areas from astronomy to biological cell imaging. Here, we investigate nanoparticle growth in situ. This optical investigation of particle growth in real time provides insight into the second part of gold nanorod synthesis, where particle growth is preferentially into the direction of the short axis, yielding more and more spherical particles. By converting the measured single-particle spectra into particle geometry using a theoretically derived transfer function, we deduce absolute values for particle geometry at each point in time. These values will provide basic input data to compare quantitatively theoretical models of nanoparticle growth.

Acknowledgment. Excellent technical help was provided by Rudolf Würfel and Georg Conrad. Furthermore, we thank Andreas Köhn for discussions on theoretical aspects, Yuriy

Khalavka for help with TEM imaging, Andreas Henkel for helping with the batch measurements, and we acknowledge financial support by the Deutsche Forschungsgemeinschaft (DFG) through an Emmy Noether Research Grant.

Supporting Information Available: Supplemental figures showing the stability of the setup (Figure S1), the probability of two particles within the diffraction limit of one particle (Figure S2), the continuous extinction spectra of particles growing in batch (Figure S3), and individual particle size developments (Figure S4). Table S1 lists the calculated data used for the transfer function F, which converts particle shape into resonance position E_{res} and its fwhm. This material is available free of charge via the Internet at http://pubs.acs.org.

References

(1) Perez-Juste, J.; Pastoriza-Santos, I.; Liz-Marzan, L. M.; Mulvaney, P. *Coord. Chem. Rev.* **2005**, *249*, 1870.
(2) Daniel, M. C.; Astruc, D. *Chem. Rev.* **2004**, *104*, 293.
(3) Alivisatos, A. P. *Science* **1996**, *271*, 933.
(4) Mulvaney, P. *Langmuir* **1996**, *12*, 788.
(5) Jana, N. R.; Gearheart, L.; Murphy, C. J. *Adv. Mater.* **2001**, *13*, 1389.
(6) Nikoobakht, B.; El-Sayed, M. A. *Chem. Mater.* **2003**, *15*, 1957.
(7) Jana, N. R.; Gearheart, L.; Murphy, C. J. *J. Phys. Chem. B* **2001**, *105*, 4065.
(8) Eustis, S.; El-Sayed, M. A. *Chem. Soc. Rev.* **2006**, *35*, 209.
(9) Raschke, G.; Kowarik, S.; Franzl, T.; Sönnichsen, C.; Klar, T. A.; Feldmann, J.; Nichtl, A.; Kurzinger, K. *Nano Lett.* **2003**, *3*, 935.
(10) McFarland, A. D.; Van, Duyne, R. P. *Nano Lett.* **2003**, *3*, 1057.
(11) Sönnichsen, C.; Reinhard, B. M.; Liphardt, J.; Alivisatos, A. P. *Nat. Biotechnol.* **2005**, *23*, 741.
(12) Dragnea, B.; Chen, C.; Kwak, E. S.; Stein, B.; Kao, C. C. *J. Am. Chem. Soc.* **2003**, *125*, 6374.
(13) El-Sayed, I. H.; Huang, X. H.; El-Sayed, M. A. *Nano Lett.* **2005**, *5*, 829.
(14) Yin, Y.; Alivisatos, A. P. *Nature* **2005**, *437*, 664.
(15) Wei, Z. Q.; Zamborini, F. P. *Langmuir* **2004**, *20*, 11301.
(16) Agarwal, V.; Aruna, I.; Banerjee, V.; Mehta, B. R. *Phys. Rev. B* **2006**, *74*, 035412.
(17) Petroski, J. M.; Wang, Z. L.; Green, T. C.; El-Sayed, M. A. *J. Phys. Chem. B* **1998**, *102*, 3316.
(18) Peng, Z. A.; Peng, X. G. *J. Am. Chem. Soc.* **2002**, *124*, 3343.
(19) Festag, G.; Steinbrueck, A.; Csaki, A.; Moeller, R.; Fritzsche, W. *Nanotechnology* **2007**, *18*, 015502.
(20) Liu, G. L.; Yin, Y. D.; Kunchakarra, S.; Mukherjee, B.; Gerion, D.; Jett, S. D.; Bear, D. G.; Gray, J. W.; Alivisatos, A. P.; Lee, L. P.; Chen, F. Q. F. *Nat. Nanotechnol.* **2006**, *1*, 47.
(21) Murphy, C. J.; San, T. K.; Gole, A. M.; Orendorff, C. J.; Gao, J. X.; Gou, L.; Hunyadi, S. E.; Li, T. *J. Phys. Chem. B* **2005**, *109*, 13857.
(22) Link, S.; Mohamed, M. B.; El-Sayed, M. A. *J. Phys. Chem. B* **1999**, *103*, 3073.
(23) Sönnichsen, C.; Franzl, T.; Wilk, T.; von Plessen, G.; Feldmann, J.; Wilson, O.; Mulvaney, P. *Phys. Rev. Lett.* **2002**, *88*, 077402.
(24) Prescott, S. W.; Mulvaney, P. *J. Appl. Phys.* **2006**, *99*, 123504.
(25) Sönnichsen, C.; Alivisatos, A. P. *Nano Lett.* **2005**, *5*, 301.
(26) Sönnichsen, C. *Plasmons in Metal Nanostructures*; Cuvillier Verlag Göttingen: München, 2001; 3-89873-235-5.
(27) Hanley, Q. S.; Verveer, P. J.; Jovin, T. M. *Appl. Spectrosc.* **1998**, *52*, 783.
(28) Jiang, S. H.; Walker, J. G. *Opt. Commun.* **2005**, *256*, 35.
(29) Liu, G. L.; Doll, J. C.; Lee, L. P. *Opt. Express* **2005**, *13*, 8520.
(30) Gemperlein, R. *Microchim. Acta* **1988**, *94*, 353.
(31) Herrala, E.; Okkonen, J. *Int. J. Pattern Recognit. Artif. Intell.* **1996**, *10*, 43.
(32) Kim, M. S.; Chen, Y. R.; Mehl, P. M. *Trans. ASAE* **2001**, *44*, 721.
(33) Muskens, O. L.; Del Fatti, N.; Vallee, F.; Huntzinger, J. R.; Billaud, P.; Broyer, M. *Appl. Phys. Lett.* **2006**, *88*.
(34) Boleininger, J.; Kurz, A.; Reuss, V.; Sönnichsen, C. *Phys. Chem. Chem. Phys.* **2006**, *8*, 3824.
(35) Novo, C.; Gomez, D.; Perez-Juste, J.; Zhang, Z. Y.; Petrova, H.; Reismann, M.; Mulvaney, P.; Hartland, G. V. *Phys. Chem. Chem. Phys.* **2006**, *8*, 3540.
(36) Draine, B. T.; Flatau, P. J. *DDSCAT*, version 6.1; 2004, http://www.astro.princeton.edu/~draine/DDSCAT.6.1.html.
(37) Johnson, P. B.; Christy, R. W. *Phys Rev B* **1972**, *6*, 4370.
(38) Link, S.; El-Sayed, M. A.; Mohamed, M. B. *J. Phys. Chem. B* **2005**, *109*, 10531.
(39) Bohren, C. F.; Huffman, D. R. *Absorption and Scattering of Light by Small Particles*; Wiley-Interscience: New York, 1983.

NL070627G